Analytical Methods

PAPER

View Article Online
View Journal | View Issue

Cite this: *Anal. Methods*, 2017, **9**, 6801

A self-supported electrochemical sensor for simultaneous sensitive detection of trace heavy metal ions based on PtAu alloy/carbon nanofibers

SongGe Zhang, Han Zhu,* PiMing Ma, Fang Duan, WeiFu Dong and MingLiang Du*

The key issue in efficient electrochemical detection of trace heavy metal ions (HMIs) is to design hierarchical nanostructure electrodes with high sensitivity and low detection limit. In this study, bimetallic PtAu alloy nanoparticles (PtAuNPs) with uniform size and distribution were constructed in electrospun carbon nanofibers (CNFs) by combining an electrospinning procedure and an *in situ* thermal reduction process. The PtAu/CNF membrane can be directly used as a sensor electrode for simultaneous detection of trace Cd^{2+}, Pb^{2+}, and Cu^{2+} by square wave anodic stripping voltammetry (SWASV). The prepared PtAu/CNF membrane is capable of simultaneously detecting Cd^{2+}, Pb^{2+}, and Cu^{2+} with a sensitivity of 0.10 μM and correlation coefficients of 0.976, 0.993, and 0.976, respectively, indicating high sensitivity and good linear relation. The excellent sensitivity and low detection limit for HMI detection were ascribed to the high conductivity of CNFs, fast response of PtAu alloy NPs, and high specific surface area of the hybrid structure. The present research provides a convenient and efficient way to construct new sensors for simultaneous trace detection of HMIs.

Received 16th September 2017
Accepted 14th November 2017

DOI: 10.1039/c7ay02223a

rsc.li/methods

1. Introduction

Heavy metal pollutants such as Cd, Pb, Cu, and Hg are known to have adverse effects on the immune, central nervous, reproductive, and developmental systems of human beings even at very low levels due to their high toxicity, hard biodegradability, and accumulation in food chain.[1–3] The research on the detection of heavy metal ions (HMI) is focussed predominantly on relevant remediation and detection technologies. Many efforts have been made to develop an efficient technique for monitoring heavy metals in the environment. A wide variety of detection technologies, such as inductively coupled plasma-mass spectrometry (ICP-MS), atomic absorption spectroscopy (AAS), X-ray fluorescence (XRF) spectrometry, atomic fluorescence spectrometry (AFS), and atomic emission spectrometry (AES), have been developed for the detection of toxins.[4–8] The main drawbacks of these techniques include expensive apparatus and time-consuming operating procedures, which are difficult to overcome for *in situ* analysis in practical applications. In addition, due to the coexisting nature of HMIs, the simultaneous detection of heavy metal ions with high sensitivity and selectivity still remains a challenging task.

In this regard, electrochemical sensors based on the square wave anodic stripping voltammetry (SWASV) method have been proven to be a powerful, portable, facile, and cost-effective technology.[8–10] Moreover, superior sensitivity and selectivity make it a preferred technique for the detection of trace heavy metal ions (HMIs).[11] Generally, SWASV includes deposition and stripping processes. Deposition is a process in which target ions are reduced to metals, whereas stripping is a process in which metals are oxidized to ions.[12–14] An extraordinary electrode material for HMI detection should have the properties of rapid HMI collection and fast electron transport. Incorporation of nanomaterials and nanostructures into sensors leads to significant improvement in the performance of electrochemical sensors in terms of sensitivity, selectivity, multiplexed detection capability, and portability.[15–18]

Nanostructure-modified electrodes possess higher surface area, improved electron transfer rate, increased mass-transport rate, lower solution resistance, and higher signal-to-noise ratio.[19–21] It has been reported that the Au NP-modified glassy carbon electrodes (GCE) would eliminate the memory effect and interferences of other ions from intermetallic compounds, thus significantly lowing the limit of detection towards Hg^{2+}.[13] Moreover, carbonaceous nanomaterials, such as carbon nanotubes (CNTs) and graphene, are perfect candidates to support metal nanocrystals due to their larger specific surface area, high conductivity, and fast mass transfer rates, which are beneficial for charge transfer and adsorption of HMIs.[22–24] Among various carbonaceous nanomaterials, electrospun carbon nanofibers (CNFs) are a suitable support for the loading of nanostructures and deposition of analyst ions due to their impressive length to

Key Laboratory of Synthetic and Biological Colloids, Ministry of Education, School of Chemical and Material Engineering, Jiangnan University, Wuxi 214122, P. R. China. E-mail: zhysw@jiangnan.edu.cn; du@jiangnan.edu.cn

diameter ratio and attractive conductivity. In addition, our group has synthesized various metals, transition metals, and transition metal sulfide nanocrystals using carbon nanofibers as nanoreactors and hosts, and these nanocrystals exhibit superior electrocatalytic activity.[25–27]

In this study, we have designed an electrochemical sensor based on a binary metal PtAu alloy nanoparticle carbon nanofiber hybrid (PtAu/CNF) for the efficient detection of trace HMIs. The PtAu/CNF hybrid membrane can be directly used as a self-supported working electrode, and it can entirely avoid the tedious process of preparation of modified electrodes such as glass carbon electrodes and screen-printed carbon electrodes. Most of the recent research on electrochemical sensors is dedicated to the detection of individual metal ions.[28–31] There are only a few studies on simultaneous electrochemical detection using binary metal nanoparticles with hierarchical nanostructures due to the difficulty in finding a suitable hierarchical unit having overall deposition potential allowing the simultaneous detection of several elements. Therefore, it is of great significance to develop electrochemical sensors based on binary metal nanomaterials for simultaneous detection of several trace metal ions. The PtAu/CNF membrane exhibited perfect variability, excellent sensitivity, and strong ability to simultaneously analyze several heavy metal ions such as Cd^{2+}, Pb^{2+}, and Cu^{2+}. For the SWASV methods, the ability to dynamically assess low-metal concentrations in aqueous solutions is critical for highly efficient detection of trace heavy metal ions. Therefore, in the present investigation, a new approach has been proposed for the detection of heavy metal ions, which has great potential in the field of real-time practical applications.

2. Experimental

2.1 Materials

Chloroauric acid ($HAuCl_4 \cdot 4H_2O$, 99.9%) and chloroplatinic acid ($H_2PtCl_6 \cdot 6H_2O$, 99.9%) were purchased from Shanghai Civi Chemical Technology Co., Ltd. Polyacrylonitrile (PAN, $M_w \approx 1.4 \times 10^5$, copolymerized with 10 wt% methyl acrylate) was purchased from Sinopec Shanghai Petrochemical Co., Ltd. *N*,*N*′-Dimethylformamide (DMF) was acquired from Shanghai Shenbo Chemical Co., Ltd (China). The Nafion aqueous solution (5 wt%) was purchased from Aldrich Chemistry Co., Ltd. $Cd(NO_3)_2 \cdot 4H_2O$, $Pb(NO_3)_2$, $CuCl_2 \cdot 2H_2O$, $K_3Fe(CN)_6$, and other reagents were obtained from Aladdin Chemical Reagent Co., Ltd. (Shanghai, China). Herein, all the reagents were used as received without further purification.

2.2 Preparation of the electrospun PtAu precursor PAN hybrid nanofiber membrane

In a typical synthesis of the precursor solution, 1.5 g of the PAN powder was first dissolved in 10 mL DMF. Then, the mixture was transferred into a 25 mL conical flask (fitted with a magnetic stirrer) and heated to 60 °C for 2 h under vigorous stirring. After 1 h, 0.050 g of chloroplatinic acid and 0.075 g chloroauric acid were slowly added to the PAN solution under continuous magnetic stirring for 1 h. To prepare the electrospun PtAu precursor PAN hybrid nanofiber membrane, the prepared precursor solution was transferred into a syringe with a capacity of 10 mL and an inner diameter of 0.8 mm. The positive voltage of a voltmeter connected with the tip of the syringe was approximately 18 kV, the negative voltage of a voltmeter connected with the rotating drum was approximately 0.5 kV, and the distance from the tip to the rotating drum was 12 cm. The feeding rate of the precursor solution was 0.6 mL h^{-1}. The PtAu precursor PAN nanofiber membrane was preserved in a vacuum drying oven for further treatment. All the experiments were performed at room temperature.

2.3 Preparation of the PtAu alloy NPs in carbon nanofibers

The PtAu/CNF hybrids were prepared by an *in situ* reduction approach. In detail, the prepared electrospun PtAu precursor PAN nanofibrous mat (20 × 20 mm) was carefully put in a home-built chemical vapor deposition (CVD) tube furnace for heat treatment. The furnace was first heated at 280 °C under an air atmosphere at a heating rate of 5 °C min^{-1} for 3 h (pre-oxidation process). Then, the membrane was heated to 1000 °C at the heating rate of 5 °C min^{-1} for 5 h under an Ar/NH_3 atmosphere (graphitization process). After continuous graphitization for 5 h, the prepared samples were cooled to room temperature in Ar/NH_3 atmosphere.

2.4 Fabrication of a PtAu/CNF-modified glass carbon electrode (PtAu/CNF/GCE)

Typically, 3 mg of PtAuNP/CNFs were added to a solution consisting of 3 : 1 (v/v) isopropanol/distilled water and 30 μL of Nafion solution (5 wt%), and then, the mixture was stirred to obtain a homogeneous ink. On the other hand, ahead of modification, the bare GCE was ultrasonically processed in ethanol for 25 min to remove the surface residue and then sequentially polished with 0.3 and 0.05 μm of alumina slurry carefully, followed by rinsing in ethanol and ultra-pure water. Finally, 5 μL of the prepared ink was carefully dropped onto the fresh GCE and dried at room temperature overnight. After solvent evaporation, the abovementioned modified electrodes were fabricated and denoted as PtAu/CNF/GCE and stored in a vacuum drying oven before further characterization.

2.5 Instrument

The morphology of the PtAuNP/CNF membrane was investigated by a field-emission scanning electron microscope (FE-SEM, JEOL, JSM-6700F, Japan) with an acceleration voltage of 3 kV. The corresponding transmission electron microscopy (TEM) images were obtained by a transmission electron microscope (JEOL, JSM-2100, Japan) with an acceleration voltage of 200 kV. X-ray diffraction (XRD) patterns of the PtAuNP/CNF hybrid were analyzed by an X-ray diffractometer (Bruker AXS D8 DISCOVER) with Cu K_α radiation ($\lambda = 1.5406$ Å, scanning rate of 0.02° 2θ s^{-1}). The X-ray photoelectron spectra of the PtAuNP/CNF membrane were obtained by an X-ray photoelectron spectrometer (XPS, Kratos Axis Ultra DLD) operated at 15 kV and 10 mA with an aluminum K_α source (1486.6 eV).

2.6 Electrochemical measurements

Electrochemical measurements were performed using a CHI660E electrochemical workstation (ChenHua Instruments Co., Shanghai, China). Cyclic voltammograms (CV) were obtained in a neutral solution of 5 mM $K_3[Fe(CN)_6]$ and determined in the potential ranged from −0.2 to 1.5 V (*vs.* SCE) at a scan rate of 100 mV s^{-1}. Square wave anodic stripping voltammetry (SWASV) was applied to detect Cd^{2+}, Pb^{2+}, and Cu^{2+} ions. The modified GCE (PtAu/CNF/GCE), platinum wire, and saturated calomel electrode (SCE) were used as the working electrode, counter electrode, and reference electrode, respectively. Herein, the three electrodes were immersed in a solution containing one or more HMI and 0.1 mol L^{-1} of NaAc–HAc (pH = 5.8). Then, the ions were reduced to the corresponding metals and deposited on the surface of the working electrode at the potential of −2.1 V *vs.* SCE for 240 s, followed by another oxidation process, namely stripping: the reduced metals transformed into their ions. All the experiments were performed under the following conditions: the amplitude, increment potential and frequency were 50 mV and 4 mV and 15 Hz, respectively. A positive potential was necessarily applied for 120 s to remove the deposited residual species from the electrode surface after each test. The PtAuNP/CNF/GCE was used to determine heavy metal ions under a relative actual water atmosphere. Moreover, other external conditions of each experiment remained unchanged to ensure comparability.

3. Results and discussion

3.1 Characterization of the PtAuNP/CNF hybrids

The PtAu/CNF hybrids were synthesized *via* a traditional electrospinning and *in situ* reduction process. The FE-SEM images of the as-prepared PtAu/CNF hybrids are shown in Fig. 1a and b. The typical CNFs are randomly distributed, and there are larger amounts of PtAu NPs uniformly immobilized on the surfaces of the CNFs. The PtAu/CNFs have uniform size distribution with an average diameter of approximately 324 ± 21 nm. The TEM images of the as-prepared PtAu/CNF hybrids are illustrated in Fig. 1c and d. It can be easily observed that the small and uniform PtAu NPs are distributed on the surface of CNFs. The HRTEM image of the PtAu NPs in Fig. 1e clearly exhibits well-defined lattice fringes with the interplanar spacing distances of 0.237 and 0.193 nm, corresponding to the (111) and (200) crystal planes of the PtAu alloy.[32,33] Additionally, the PtAu NPs were coated with several carbon layers, and the average diameter of the PtAu NPs ranged from 4 to 16 nm. As shown in Fig. 1f, a typical selected area electron diffraction pattern (SAED) of PtAu/CNF hybrids indicates the concentric diffraction rings, suggesting the polycrystallinity of the PtAu NPs.

Fig. 2 displays the chemical composition and elemental distribution of PtAu/CNFs investigated by scanning transmission electron microscopy (STEM) characterization. As shown in the HAADF-STEM image in Fig. 2a, the PtAu NPs are uniformly distributed on the surfaces of CNFs. The STEM-EDS mapping images of the PtAu/CNFs clearly exhibit four elements: carbon, nitrogen, platinum, and gold. Carbon and nitrogen belong to the CNFs, indicating N-doped carbon. Moreover, the consistent position of Pt and Au elements further confirms the homogeneous distribution and the homogeneous phase structure of PtAu NPs. The STEM image and line scan STEM-EDX spectra shown in Fig. 2c and d strongly demonstrate the uniform distribution of Pt and Au around the four PtAu alloy NPs. All the abovementioned results further confirmed the successful fabrication of the PtAu/CNF hybrids.

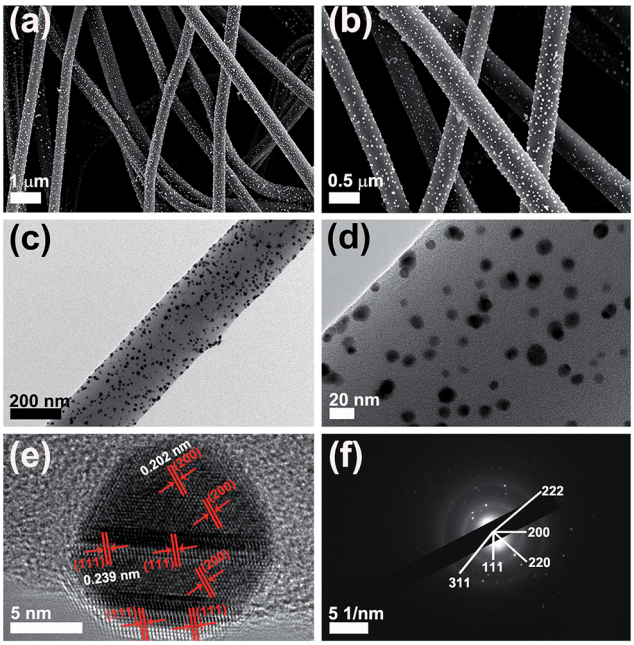

Fig. 1 (a and b) FE-SEM images of the as-prepared PtAu/CNFs. (c and d) TEM image of the PtAu/CNFs. (e) HRTEM image and (f) SAED pattern of the PtAu NPs.

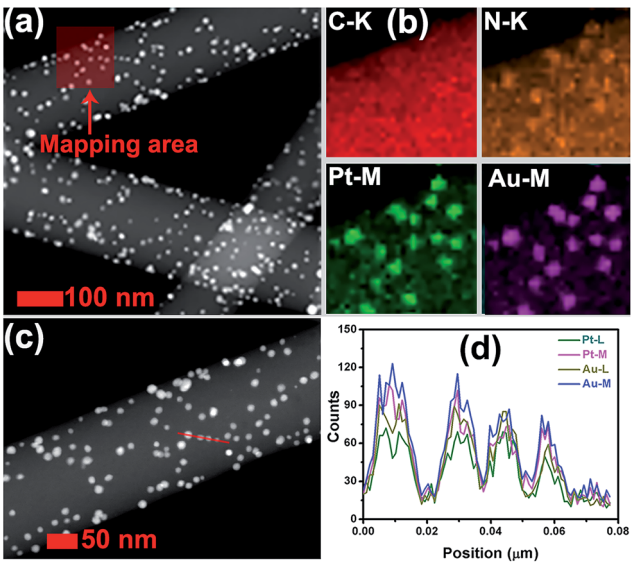

Fig. 2 (a) HAADF-STEM and (b) STEM-EDS mapping images of the PtAu/CNF hybrids. (c, d) The line-scanned area and the EDX spectrum of the PtAu/CNFs hybrids.

As illustrated in Fig. 3, the XRD pattern of the PtAu/CNF hybrids further provides more structural information. For the PtAu/CNF hybrids, four representative diffraction peaks emerged at 38.3°, 44.4°, 64.8°, and 77.8°, which were distinctly assigned to the (111), (200), (220), and (311) planes of the fcc structure of the PtAu alloy, respectively.[32,33] Compared to the strong and sharp representative diffraction peaks, it is worth noting that a broad diffraction peak has been detected at $2\theta = 24.7°$ in the PtAu/CNFs, which is ascribed to the crystalline structure and amorphous phase of the graphitic carbon ((002) plane) in the carbon nanofibers. The abovementioned results confirmed the favorable crystallization of PtAuNPs, amorphous phase of graphitic carbon of the CNFs, and the formation of PtAu/CNFs.

To further study the surface chemical states of the PtAu alloy, the XPS spectra of the PtAu/CNF hybrid are demonstrated in Fig. 3. Fig. 3b displays the C 1s XPS spectra, and there are three representative peaks located at 284.8, 285.8, and 289.3 eV, which are attributed to the C–C, C–O, and O–C═O groups, respectively.[34] As shown in Fig. 3b, there are two sharp and identifiable peaks emerging at 71.2 and 75.3 eV, which are associated with the binding energies (BEs) of Pt $4f_{7/2}$ and Pt $4f_{5/2}$, respectively.[31–33] The Au 4f spectra exhibit two strong peaks emerging at 84.3 and 87.9 eV, corresponding to the BEs of Au $4f_{7/2}$ and Au $4f_{5/2}$.[31–33] Moreover, there are no other peaks, and the predominant Pt^0 and Au^0 4f peaks confirmed the successful synthesis of the PtAu alloy. It can be concluded that PtAu existed in metallic state in the PtAu/CNF hybrids. The abovementioned observations are consistent with the FE-SEM and XRD results.

3.2 Electrochemical performance characterization of the PtAuNP/CNF hybrids

To investigate the electrochemical activity of the PtAu/CNF hybrids, the CV response of the bare GCE, CNFs, and PtAuNP/CNF-modified GCE were obtained in a solution of 5 mM $K_3[Fe(CN)_6]$ at a scan rate of 100 mV s^{-1}. The potential ranged from −1.4 to 1.2 V (*vs.* SCE), as shown in Fig. 4a. The CVs of PtAu/CNF/GCE show a couple of well-defined redox peaks as compared to those of the bare GCE; this indicates that the combination of PtAu NPs and CNFs can effectively accelerate the electron transfer. The CNF/GCE has no redox peak; this indicates that the PtAu NPs can enhance the electron transfer. The improved effective active area of the modified PtAu/CNF electrode implied an effective conduction pathway and a favourable electrochemical behaviour, which was attributed to the strong adsorptive properties of the PtAu/CNF hybrids. The SWASV response indicates that the four considered heavy metal ions can be detected in well-separated stripping peaks, which can realize the simultaneous detection. It is thus easy to distinguish four heavy metal ions from the potential of the stripping peak using the PtAu/CNF-modified electrode.

To further confirm the extraordinary electrochemical behaviour, Fig. 4b shows the SWASV signals of the bare, CNF/GCE, and PtAu/CNF/GCE in the solution containing 2 μM Cd^{2+}, Pb^{2+}, and Cu^{2+} ions. For the simultaneous detection of Cd^{2+}, Pb^{2+}, and Cu^{2+}, the bare GCE exhibited three weak peaks in the stripping process. By contrast, the PtAu/CNF/GCE exhibited three well-defined peaks with higher peak current and more stable base line than those obtained for the CNF/GCE. All these observations indicate the excellent electrochemical behaviour of the PtAu/CNF/GCE, especially for simultaneous detection.

3.3 Electrochemical detection of a single heavy metal ion with the PtAu/CNF membrane

Based on the excellent electrocatalytic properties of PtAu/CNF/GCE, the PtAu/CNF membrane can be directly used as a self-supported electrochemical sensor for the detection of trace heavy metal ions. In a follow-up experiment, the PtAu/CNF membrane was directly used as a working electrode for the detection of different heavy metal ions. As shown in Fig. 5a, c, and e, the SWASV responses for the detection of 1.0 μM Cd^{2+}, Pb^{2+}, and Cu^{2+} ions were obtained, respectively, which were

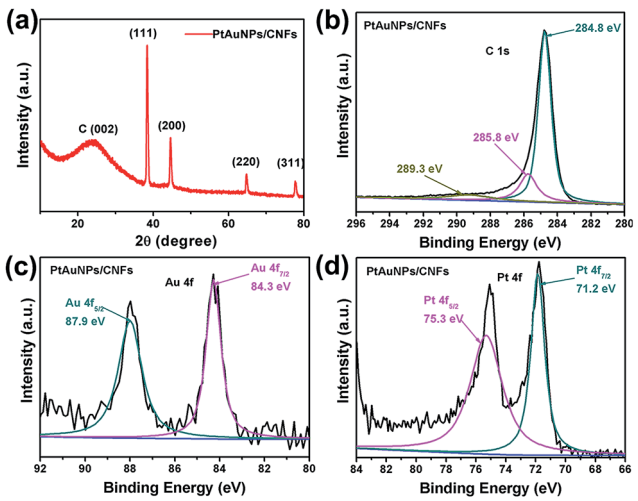

Fig. 3 (a) XRD pattern of the PtAu/CNFs. High resolution (b) C 1s, (c) Pt 4f, and (d) Au 4f XPS spectra of the PtAu/CNF hybrids. The XPS spectra marked as black are the original results, and coloured spectra are the deconvoluted results. XRD and XPS results demonstrated the formation of PtAu NPs supported on the CNFs.

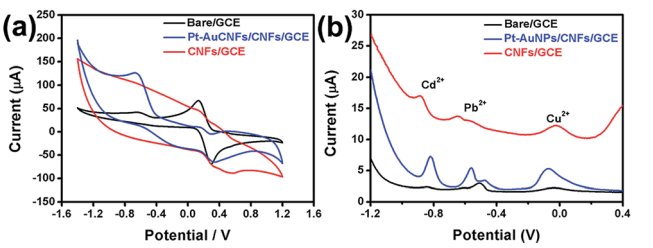

Fig. 4 (a) Cyclic voltammograms obtained in 5 mM $K_3[Fe(CN)_6]$ solutions using bare GCE, CNF/GCE, and PtAu/CNF/GCE as electrodes. Scan rate, 100 mV S^{-1}. (b) SWASV response towards Cd(II), Pb(II), and Cu(II) detection on GCE, CNF/GCE, and PtAu/CNF/GCE electrodes in a 0.1 M acetate buffer solution containing 2 μM of Cd^{2+}, Pb^{2+}, and Cu^{2+} is 2 μM (pH = 5.8) at the deposition potential of −1.8 V for 180 s. The potential step is 4 mV, the amplitude is 50 mV, and the frequency is 15 Hz.

acquired over a series of deposition time (60–300 s) and deposition potential of −1.5 V. Generally, the stripping peak current exhibited an up trending and linear growth with the increasing deposition time, except for Cd^{2+}. This can be attributed to the difference in adsorption and desorption behaviours for different metal ions, leading to the huge influence in the stripping process. Moreover, in the deposition at −1.8 V (Fig. 5b, d, and f), the general trend remained unchanged, and the stripping peak changed for Pb^{2+}; this was ascribed to the increased deposition and the variation of desorption properties. The stripping peak potential of Cd^{2+}, Pb^{2+}, and Cu^{2+} was approximately −0.78 V, −0.56 V, and 0 V, respectively, suggesting the simultaneously detection.

3.4 Electrochemical detection of double heavy metal ions with the PtAu/CNF membrane

As shown in Fig. 6, the SWASVs response over a deposition time (60–300 s) and different deposition potentials for simultaneous detection of 1.0 μM Cd^{2+}, Pb^{2+} and Pb^{2+}, Cu^{2+} was achieved, and the overall peak shape was obtained. In the simultaneous detection of 1.0 μM Cd^{2+} and Pb^{2+} (Fig. 6a, c, and e), the two corresponding stripping peaks become sharp, and the current gradually increases with the increasing deposition time. However, when the deposition potential increased to −1.8 V, the current of the stripping peak could maintain the linear growth; this suggested that the potential was enough for the saturation of adsorbed ions. For the simultaneous detection of Pb^{2+} and Cu^{2+} (Fig. 6b, d, and f), the peak current exhibits a better linear growth with the increasing deposition time. Similarly, when the deposition potential increased to −1.8 V, the stripping peak current of Pb^{2+} showed no difference until the deposition time increased to 300 s. This indicates that only when the deposition time increases to a certain value, the peak current can increase with the increasing deposition potential.

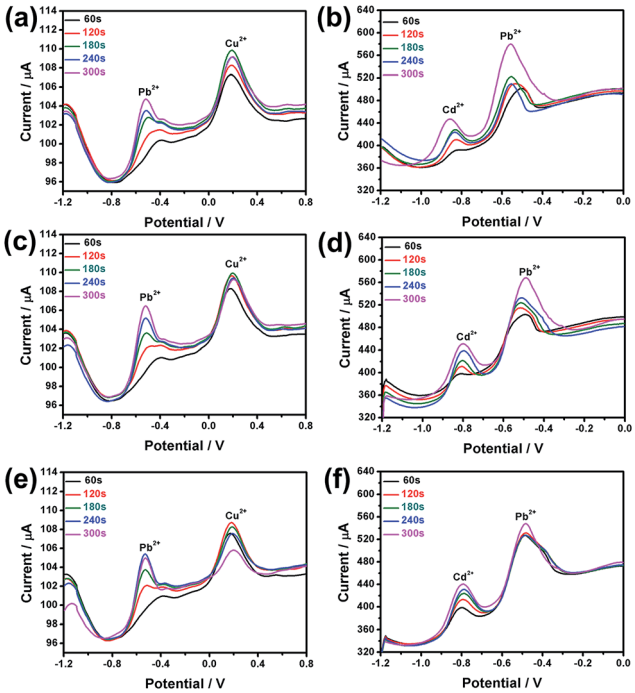

Fig. 6 SWASVs for simultaneous detection of 1.0 μM Cd^{2+}, Pb^{2+} and Pb^{2+}, Cu^{2+} with the PtAuNP/CNF film over a deposition time (60–300 s) and deposition potential of −1.2 V (a and b), −1.5 V (c and d), and −1.8 V (e and f).

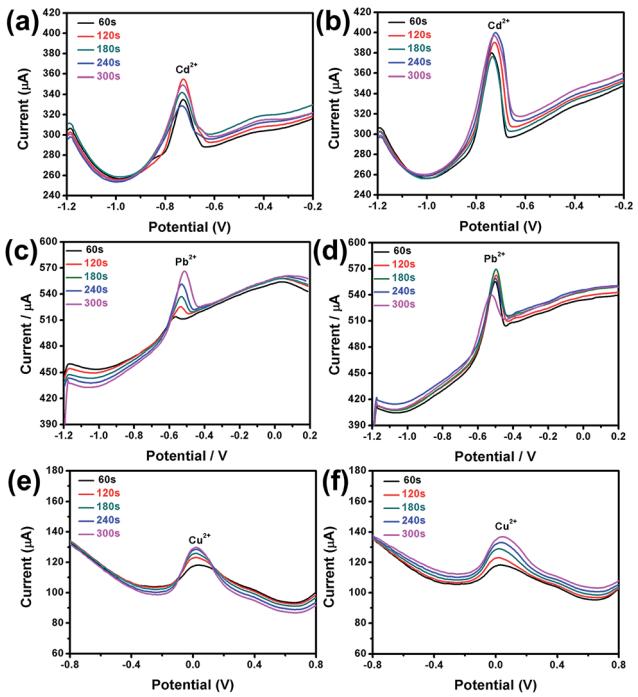

Fig. 5 SWASVs for the detection of 1.0 μM Cd^{2+}, Pb^{2+}, and Cu^{2+} obtained by the PtAuNP/CNF membrane over a series of deposition time (60–300 s) and deposition potential of −1.5 V (a, c, and e) and −1.8 V (b, d, and f) in a 0.1 M acetate buffer solution.

3.5 Experimental parameter optimization of simultaneous detection of heavy metal ions with the PtAu/CNF membrane

A series of experiments for the simultaneous detection of Cd^{2+}, Pb^{2+}, and Cu^{2+} was performed. As shown in Fig. 7, all the experiments were carried out in an acetate buffer solution containing 1 μM of Cd^{2+}, Pb^{2+}, and Cu^{2+}. For the detection of trace heavy metal ions, it is necessary to optimize the experimental parameters to obtain a higher sensitivity and lower

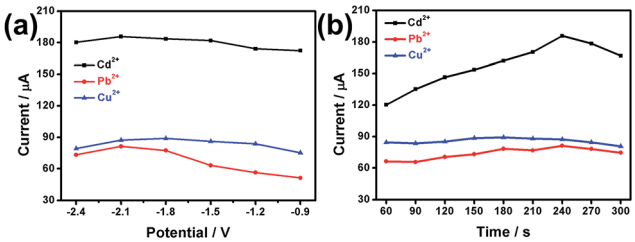

Fig. 7 The experimental parameter optimization of deposition potential (a) and deposition time (b). All data were obtained by SWASV detection of metal ion solution containing 1.0 μM each of Cd^{2+}, Pb^{2+}, and Cu^{2+}.

detection limit. Fig. 7a demonstrates the influence of deposition potential on the response of different HMIs. The stripping currents of Cd^{2+}, Pb^{2+}, and Cu^{2+} exhibit a trend such that the current of HMI increases first and then decreases with an increase in potentials from −0.9 V to −2.4 V. It is obvious that the deposition potential of −2.1 V is the optimal potential. It is ascribed to the insufficient accumulation of ions at lower potentials, and the occurrence of hydrogen evolution reaction at higher potentials. Therefore, the potential of −2.1 V was used as the optimum deposition potential for the simultaneous detection of Cd^{2+}, Pb^{2+}, and Cu^{2+} ions.

The simultaneous detection of Cd^{2+}, Pb^{2+}, and Cu^{2+} by SWASV is demonstrated in Fig. 8. In detail, the simultaneous detection of 0.1 μM and 0.25 μM HMI ions was performed in 0.1 M HAc–NaAc with 1 μM Bi^{3+} ion, which is shown in Fig. 8a and b. The detection of 0.5 μM and 1.0 μM HMI ions was performed without Bi^{3+}, as shown in Fig. 8c and d, respectively. Fig. 8 exhibits three well-defined and well-separated stripping peaks corresponding to Cd^{2+}, Pb^{2+}, and Cu^{2+} at different concentrations varying from 0.1 μM to 1.0 μM, indicating the excellent adsorption and desorption properties of the multiple target ions. The relatively higher concentration, especially 1.0 μM HMI, displays relative stronger peaks, and the peak shape tends to close and be ambiguous at low concentrations; this is ascribed to the insufficiency of the stripping process. However, the prepared self-supported PtAu/CNF membrane electrode displays effective simultaneous detection of Cd^{2+}, Pb^{2+}, and Cu^{2+} in 0.1 μM; this demonstrates the extraordinary sensibility and low detection limit.

As shown in Fig. 9, to further investigate the linear range of simultaneous detection, the SWASVs for the simultaneous detection of Cd^{2+}, Pb^{2+}, and Cu^{2+} at different concentrations were obtained to determine the linear relationship. The three stripping peaks at the potential of −0.79, −0.48, and 0.09 V correspond to the oxidation potential of Cd, Pb, and Cu, respectively. The fitting curves of the linear relationship

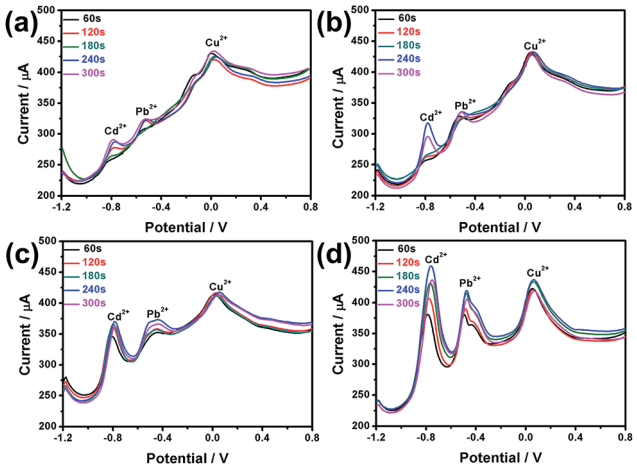

Fig. 8 SWASVs for simultaneous detection of Cd^{2+}, Pb^{2+}, and Cu^{2+} over a deposition time (30–300 s) in 0.1 M HAc–NaAc and metal ion solution at different concentrations: (a) 0.1 μM, (b) 0.25 μM, (c) 0.5 μM, and (d) 1.0 μM.

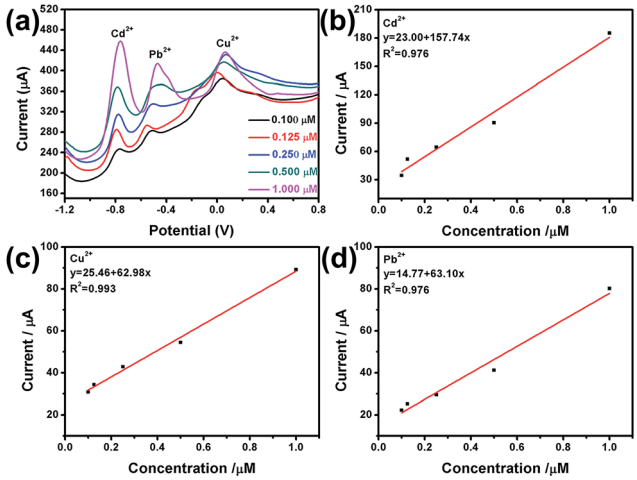

Fig. 9 (a) SWASVs for the simultaneous detection of Cd^{2+}, Pb^{2+}, and Cu^{2+} at different concentrations; (b–d) the corresponding calibration curve plots of Cd^{2+}, Pb^{2+}, and Cu^{2+} ions.

between the peak current and ion concentration are shown in Fig. 9b–d, corresponding to Cd^{2+}, Pb^{2+}, and Cu^{2+}. It is obvious that the currents become higher with the increasing ion concentrations, and the calibration curves are linear in the range from 0.1 to 1.0 μM for all the three target ions. The correlation coefficients of the linearization equations were 0.976, 0.993, and 0.976, respectively, indicating the high sensitivity and good linear relation of the PtAuNPs/CNF hybrids. From Table 1, the relative standard deviations (RSD) of the as-prepared sensor for each ions were measured with 5 reduplicative experiments. The RSDs in both 0.5 μM and 1.0 μM exhibit relative small values, indicating that the self-supported PtAuNP/CNF membrane can be applied to detect heavy metal ions simultaneously with high repeatability.

The electrochemical sensor based on the self-supported PtAuNP/CNF membrane exhibited excellent sensitivity and low detection limit; this is attributed to the high conductivity of CNFs and the quick response of PtAu alloy NPs to target ions.

The high electron transport capability of CNFs can facilitate the stripping and deposition of heavy metal ions, and the excellent stability of CNFs will endow the electrode with good durability. The PtAu/CNFs exhibit a high surface-specific area and high porosity, which are beneficial for the penetration of heavy metal-ion solutions. Moreover, the PtAu/CNF membrane was directly used as a working electrode for the determination of heavy metal ions, along with excellent durability of the hybrids provided by CNFs. Therefore, the present research provides a convenient and efficient way for simultaneous and sensitive detection of trace heavy metal ions.

Table 1 The stability of the as-prepared PtAuNP/CNF hybrid film

Concentration	RSD for Cd^{2+}	RSD for Pb^{2+}	RSD for Cu^{2+}
0.5 μM	4.32%	6.76%	6.23%
1.0 μM	5.14%	7.56%	7.42%

4. Conclusions

In summary, an extraordinary electrode material was fabricated *via* an electrospinning procedure and *in situ* thermal reduction process. The PtAu/CNF hybrids consist of well-dispersed PtAu alloy NPs and homogeneous CNFs with excellent sensitivity and low detection limit for trace heavy metal ions. The PtAu/CNF film was directly used as a working electrode for simultaneous or individual detection of Cd^{2+}, Pb^{2+}, and Cu^{2+} by the SWASV methods. The PtAu/CNF membrane exhibited extraordinary electroanalytical properties. The excellent sensitivity and low detection limit of PtAu/CNF hybrids for the detection of heavy metal ions were ascribed to the high conductivity of CNFs, quick response of PtAu alloy NPs to target ions, and high specific surface area of the hybrid structure. The present research provides a convenient and efficient way to simultaneously detect trace heavy metal ions.

Conflicts of interest

There are no conflicts of interest to declare.

Acknowledgements

This study was supported by the National Natural Science Foundation of China (NSFC) (Grant no. 51373154, 51573166), the MOE & SAFEA, and 111 Project (B13025).

Notes and references

1 W. Zhang, S. Zhu, R. Luque, S. Han, L. Hu and G. Xu, *Chem. Soc. Rev.*, 2016, **45**, 715–752.
2 Q. Ji, X. An, H. Liu, L. Guo and J. Qu, *ACS Nano*, 2015, **9**, 10922–10930.
3 N. Zhang, R. Qiao, J. Su, J. Yan, Z. Xie, Y. Qiao, X. Wang and J. Zhong, *Small*, 2017, **13**, 1604293.
4 S. Wang, E. S. Forzani and N. Tao, *Anal. Chem.*, 2007, **79**, 4427–4432.
5 L. A. Hutton, G. D. O'Neil, T. L. Read, Z. J. Ayres, M. E. Newton and J. V. Macpherson, *Anal. Chem.*, 2014, **86**, 4566–4572.
6 L. Zhang, J. X. H. Wong, X. Li, Y. Li and H. Z. Yu, *Anal. Chem.*, 2015, **87**, 5062–5067.
7 Y. Hong, M. Wu, G. Chen, Z. Dai, Y. Zhang, G. Chen and X. Dong, *ACS Appl. Mater. Interfaces*, 2016, **8**, 32940–32947.
8 H. Lin, M. Li and D. Mihailovic, *Electrochim. Acta*, 2015, **154**, 184–189.
9 Q. Sun, J. Wang, M. Tang, L. Huang, Z. Zhang, C. Liu, X. Lu, K. W. Hunter and G. Chen, *Anal. Chem.*, 2017, **89**, 5024–5029.
10 J. C. Cunningham, M. R. Kogan, Y. J. Tsai, L. Luo, I. Richards and R. M. Crooks, *ACS Sens.*, 2016, **1**, 40–47.
11 Y. F. Sun, L. J. Zhao, T. J. Jiang, S. S. Li, M. Yang and X. J. Huang, *J. Electroanal. Chem.*, 2016, **760**, 143–150.
12 W. Gao, H. Y. Y. Nyein, Z. Shahpar, H. M. Fahad, K. Chen, S. Emaminejad, Y. Gao, L. C. Tai, H. Ota, E. Wu, J. Bullock, Y. Zeng, D. H. Lien and A. Javey, *ACS Sens.*, 2016, **1**, 866–874.
13 B. Zhang, J. D. Chen, H. Zhu, T. T. Yang, M. L. Zou, M. Zhang and M. L. Du, *Electrochim. Acta*, 2016, **196**, 422–430.
14 Y. Zhang, Y. Liu, X. Ji, C. E. Banksb and W. Zhang, *Chem. Commun.*, 2011, **47**, 4126–4128.
15 P. Veerakumar, V. Veeramani, S. M. Chen, R. Madhu and S. B. Liu, *ACS Appl. Mater. Interfaces*, 2016, **8**, 1319–1326.
16 P. Veerakumar, S. M. Chen, R. Madhu, V. Veeramani, C. T. Hung and S. B. Liu, *ACS Appl. Mater. Interfaces*, 2015, **7**, 24810–24821.
17 M. Yang, X. Chen, T. J. Jiang, Z. Guo, J. H. Liu and X. J. Huang, *Anal. Chem.*, 2016, **88**, 9720–9728.
18 D. A. Uygun, B. Jurado-Sánchez, M. Uygun and J. Wang, *Environ. Sci.: Nano*, 2016, **3**, 559–566.
19 J. T. Zhang, Z. Y. Jin, W. C. Li, W. Dong and A. H. Lu, *J. Mater. Chem. A*, 2013, **1**, 13139–13145.
20 X. Sun, C. Cai, T. Liu, G. Zhang, D. Cai, S. Xiong and Z. Wu, *Anal. Methods*, 2016, **8**, 303–310.
21 A. R. Rajamani, U. B. R. Ragula, N. Kothurkar and M. Rangarajan, *CrystEngComm*, 2014, **16**, 2032–2038.
22 L. H. Zhang, W. C. Li, D. Yan, H. Wang and A. H. Lu, *Nanoscale*, 2016, **8**, 13695–13700.
23 D. Chen, H. Zhu, S. Yang, N. Li, Q. Xu, H. Li, J. He and J. Lu, *Adv. Mater.*, 2016, **28**, 10443–10458.
24 J. S. Hu, L. S. Zhong, W. G. Song and L. J. Wan, *Adv. Mater.*, 2008, **20**, 2977–2982.
25 H. Zhu, L. Gu, D. Yu, Y. Sun, M. Wan, M. Zhang, L. Wang, L. Wang, W. Wu, J. Yao, M. Du and S. Guo, *Energy Environ. Sci.*, 2017, **10**, 321–330.
26 H. Zhu, J. Zhang, R. Yanzhang, M. Du, Q. Wang, G. Gao, J. Wu, G. Wu, M. Zhang, B. Liu, J. Yao and X. Zhang, *Adv. Mater.*, 2015, **27**, 4752–4759.
27 T. T. Yang, H. Zhu, M. Wan, L. Dong, M. Zhang and M. L. Du, *Chem. Commun.*, 2016, **52**, 990–993.
28 M. R. Rahman, T. Okajima and T. Ohsaka, *Anal. Chem.*, 2010, **82**, 9169–9176.
29 S. F. Zhou, X. J. Han and Y. Q. Liu, *J. Alloys Compd.*, 2016, **684**, 1–7.
30 W. H. Xu, Q. Q. Meng, C. Gao, J. Wang, Q. X. Li, J. H. Liu and X. J. Huang, *Chem. Commun.*, 2014, **50**, 5011–5013.
31 M. Li, H. Gou, I. Al-Ogaidi and N. Wu, *ACS Sustainable Chem. Eng.*, 2013, **1**, 713–723.
32 J. Zhang, G. Chen, D. Guay, M. Chaker and D. Ma, *Nanoscale*, 2014, **6**, 2125–2130.
33 M. Yin, Y. Huang, L. Liang, J. Liao, C. Liu and W. Xing, *Chem. Commun.*, 2011, **47**, 8172–8174.
34 J. N. Zheng, S. S. Li, X. Ma, F. Y. Chen, A. J. Wang, J. R. Chen and J. J. Feng, *J. Mater. Chem. A*, 2014, **2**, 8386–8395.